Supporting Information

Zero-Trigger Ultrafast Charge-Transfer J-Aggregates via Se/π-directed Assembly Enable Synchronous ROS/Heat Amplification for NIR-II Photoimmunotherapy

Dandan Ma[1#], Hui Bian[2#], Fei Pan[3], Danhong Zhou[4], Zhi Chen[5], Haoying Ge[4], Yuanlang Guo[1], Yingnan Wu[1], Xin He[1], Panwang Zhou[6], Lei Wang[1], Xiaoqiang Chen[1]* and Xiaojun Peng[1, 4]*

[1] College of Materials Science and Engineering, Shenzhen University, Shenzhen 518060, P.R. China

[2] Department of Chemistry and Nanoscience, Ewha Womans University, 03760 Seoul, Republic of Korea

[3] Institute of Apicultural Research, Chinese Academy of Ag-ricultural Sciences, Beijing 100093, P. R. China

[4] State Key Laboratory of Fine Chemicals, Frontiers Science Center for Smart Materials, Dalian University of Technology, Dalian, 116024, P.R. China

[5] College of Chemistry and Environmental Engineering, Shenzhen University, Shenzhen, Guangdong 518060, China

[6] State Key Laboratory of Catalysis, National Laboratory for Clean Energy, Dalian Institute of Chemical Physics, Chinese Academy of Sciences, Dalian, 116023, China

*Corresponding Author(s): Xiaojun Peng: pengxj@dlut.edu.cn; Xiaoqiang Chen: chenxq@szu.edu.cn

[#] These authors contributed equally

1. Synthesis

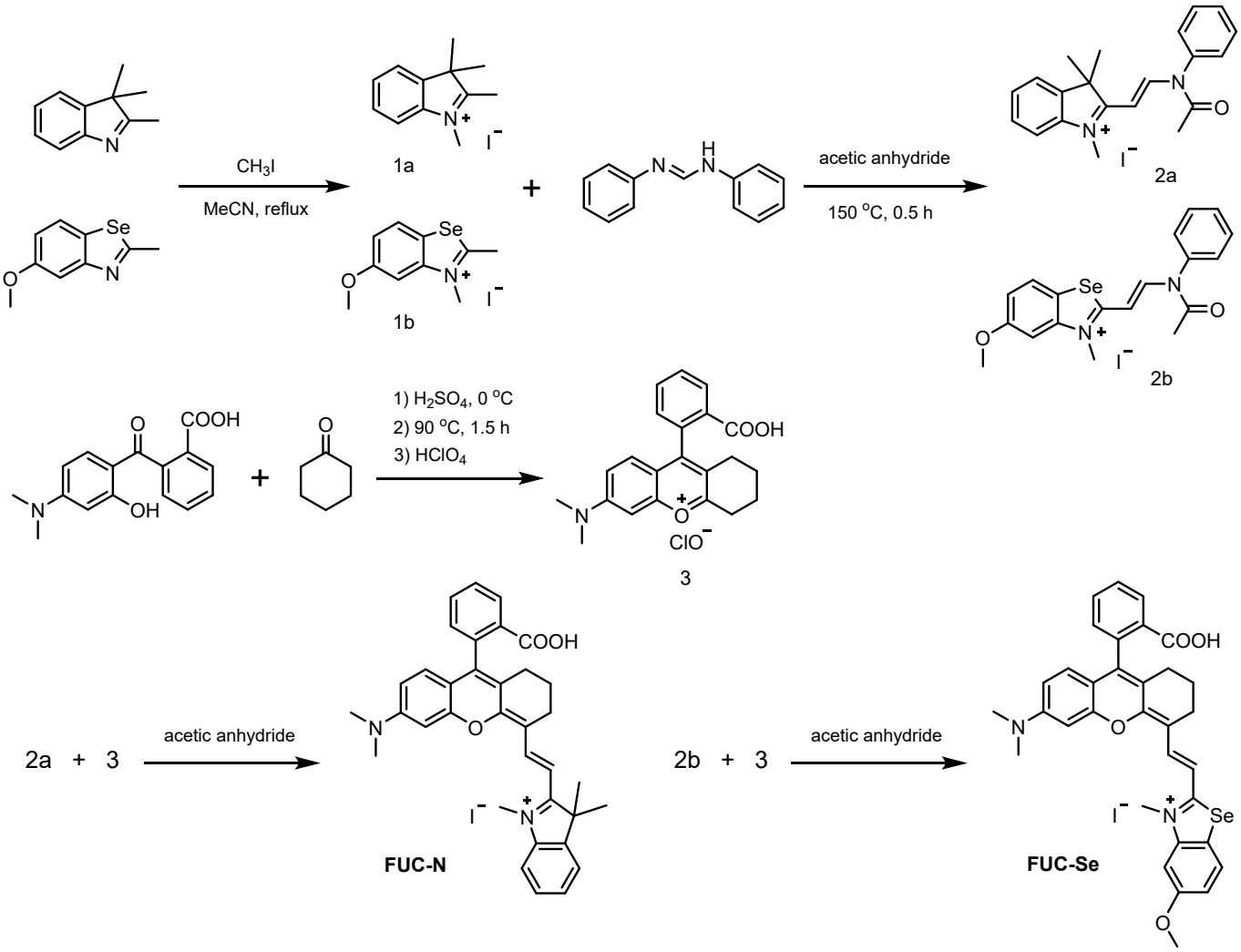

Scheme S1. Synthesis routes of **FUC-N** and **FUC-Se**.

Synthesis of Compound 1a and 1b

Methyl iodide (5 eq) is added to the solution of 2,3,3-trimethylindolenine (1 eq) or 5-methoxy-2-methylbenzoselenazole (1eq) in acetonitrile. And the reaction mixture was heated at reflux for 16 h under N_2. The resulting solid is filtered, washed with Et_2O and dried to afford crude compound 1a or 1b. The crude product was used directly in the next step without further purification.

Synthesis of Compound 2a and 2b

Compound 1a (0.92 g, 2.5 mmol) and *N*, *N*'-Diphenylmethanimidamide (0.59 g, 3 mmol) were suspended in acetic anhydride (30 mL). The suspension was stirred at 150 °C for 0.5 h. The reaction mixture was cooled to room temperature and then distilled under reduced pressure. Ethyl acetate was added to the residue, and the precipitate is filtered and dried in vacuo to give compound 2a (dark red

powder). The synthesis of compound 2b was similar that of 2a. The crude product was also used directly in the next step without further purification.

Synthesis of Compound 3

Freshly distilled cyclohexanone (6.6 mL, 63.7 mmol) was added dropwise to concentrated H_2SO_4 (70 mL) at 0 °C. Then, 2-(4-methylamino-2-hydroxybenzoyl) benzoic acid (32 mmol) was added in portions with vigorous stirring. The reaction mixture was heated at 90 °C for 1.5 h, cooled down, and poured onto ice (300 g). Perchloric acid (70%, 7 mL) was then added, and the resulting precipitate was filtered off. The crude compound 3a was obtained as a dark red solid after washed with cold water (100 mL), and was also used for the next step without further purification.

Synthesis of Compound FUC-N

Compound 2a (210 mg, 0.50 mmol) and compound 3 (350 mg,1.00 mmol) were dissolved in a mixture of CH_2Cl_2 (25 mL), CH_3OH (12 mL), and acetic anhydride (1.5 mL). The mixture is stirred for 1 h at 50 °C. The solvent was removed under reduced pressure to give the crude product, which is purified by silica gel flash chromatography using CH_2Cl_2 to CH_2Cl_2/ CH_3OH (200: 1 to 20: 1) as the eluent to afford **FUC-N** (161 mg, yield 48.8%). ^{1}H NMR (400 MHz, CD_3OD) δ 8.70 (d, J = 14.4 Hz, 1H), 8.23 (d,J = 7.0 Hz, 1H), 7.74 (d, J = 4.5 Hz, 1H), 7.67 (d, J = 4.4 Hz, 1H), 7.59–7.50 (m, 1H), 7.43 (d, J = 7.7 Hz, 1H), 7.29 (dd, J = 24.4, 6.3 Hz, 3H), 6.77 (d, J = 12.9 Hz, 3H), 6.20 (d, J = 15.0 Hz, 1H), 3.65 (s, 3H), 3.16 (s, 6H), 2.69 (s, 2H), 2.36 (s, 2H), 2.12 (d, J = 65.5 Hz, 2H), 1.83 (s, 6H). HRMS (ESI) m/z calcd for $C_{35}H_{35}N_2O_3^+$. (M-I) $^+$: 531.2642, Found 531.2625.

Synthesis of Compound FUC-Se

Compound 2a (256.62 mg, 0.50 mmol) and compound 3 (350 mg, 1.00 mmol) were dissolved in a mixture of CH_2Cl_2 (25 mL), CH_3OH (12 mL), acetic anhydride (1.5 mL), and TEA (1.5 mL). The mixture is stirred for 1 h at 50 °C. The solvent was removed under reduced pressure to give the crude product, which is purified by. It was purified by silica gel flash chromatography using CH_2Cl_2 to CH_2Cl_2/CH_3OH (200:1 to 15:1) as the eluent to afford **FUC-Se** (109 mg, yield 45.7%). ^{1}H NMR (400 MHz, $CDCl_3$) δ 8.20 (d, J = 13.2 Hz, 1H), 8.06 – 7.99 (m, 1H), 7.74 (d, J = 8.7 Hz, 1H), 7.58 – 7.50 (m, 2H), 7.13 – 7.07 (m, 1H), 7.04 (s, 1H), 6.95 (dd, J = 8.8, 2.2 Hz, 1H), 6.83 (d, J = 9.1 Hz, 1H), 6.64 (dd, J = 9.2, 2.4 Hz, 1H), 6.49 (s, 1H), 6.43 (d, J = 13.4 Hz, 1H), 3.87 (s, 3H), 3.73 (s, 3H), 3.03 (s, 6H), 2.61 (s, 2H), 2.45 (s, 1H), 2.37 (s, 1H), 1.85 (s, 1H), 1.77 (s, 1H). ^{13}C NMR (100 MHz, CD_3OD) δ 172.78, 170.45, 161.93, 160.54, 155.03, 153.83, 153.32, 144.87, 142.22, 139.60, 133.57, 129.51, 129.09, 128.56, 128.50, 128.19, 125.67, 121.11, 115.36, 114.17, 114.01, 112.98, 111.41, 101.60, 99.78, 95.64, 55.56, 39.64, 34.35, 26.56, 24.89, 20.46. HRMS (ESI) m/z calcd for $C_{33}H_{31}N_2O_4Se^+$. (M-I) $^+$: 599.1444. Found 599.1432.

2. Preparation and characterization of FUC-Se J aggregates

(1) Preparation of Sheet-like J-Aggregates (**FUC-Se**): The sheet-like J aggregates were prepared by simply adding the **FUC-Se** stock solution into an aqueous medium (ultrapure water or PBS), followed by brief mixing via pipetting. This entire process, from mixing to complete aggregate formation, consistently concluded within seconds. The assembly occurred spontaneously without any external stimulation such as heating, pH adjustment, ionic control, or sonication.

(2) Fabrication of Nanoparticulate J-Aggregates (**FUC-Se@LP**): **FUC-Se** and DSPE-PEG2000 at varying mass ratios (from 1:4 to 20:1) were dissolved in a mixture of chloroform (15 mL) and ethanol (5 mL). The solution was stirred at room temperature for 6-8 hours. The organic solvents were then removed by rotary evaporation to form a thin lipid film on the inner wall of the flask. Subsequently, 10 mL of preheated PBS (37 °C) was added to hydrate the film under sonication for 20 minutes. The resulting dispersion was extruded through 0.45 μm filters to obtain the **FUC-Se@LP** nanoparticle stock solution, which was stored at 4 °C for further use.

(3) Particle size and zeta potential test: The as-prepared nanoparticle dispersions at different mass ratios were diluted with ultrapure water prior to measurements. The hydrodynamic diameter and zeta potential of each sample were determined using a Nano ZS90 analyzer (Malvern Panalytical, UK). Each measurement was equilibrated for 2 min before data collection. To evaluate dispersion stability, the same samples were analyzed every 48 hours over a defined period.

(4) Near-infrared II fluorescence imaging: The nanoparticle dispersions were diluted 100-fold with PBS and transferred into separate centrifuge tubes labeled according to their mass ratios. The tubes were arranged in descending order of DSPE-PEG2000-to-**FUC-Se** ratio (from 1:4 to 20:1). For reference, a solution of 20 μM **FUC-Se** in 50% ethanol (v/v) was prepared and placed on the far right. NIR-II fluorescence images were acquired using an imaging system with an 808 nm excitation laser, a 900 nm long-pass emission filter (LP900), and an exposure time of 350 ms.

3. Quantum-chemical Computational Details

The ground and excited state geometries of **FUC-Se** monomer were optimized using density functional theory (DFT) and time-dependent DFT (TD-DFT) at the B3LYP/6-31g(d) level of theory. The initial model of **FUC-Se** dimmer was intercepted from the crystal structure model, and the ground and excited states were optimized using DFT and TD-DFT at the B3LYP-D3/6-31g(d) level of theory [1]. The vertical excitation of all compounds in water was calculated using TD-TDF at the B3LYP /TZVP level of theory including the polarizable continuum model (PCM) [2]. All calculations were carried out by employing the

Gaussian 16 program [3]. The spin-orbital coupling (SOC) values were calculated with ORCA 5.03 [4]. The Natural bond orbitals (NTOs) and the Hole-Electron analysis were carried out using the Multiwfn 3.8 [5].

4. Molecular Dynamic Simulation Computational Details

DSPE-PEG2000 was simplified to shorter amphiphilic molecule DSPE-PEG2. The 3D structure and topology of the DSPE-PEG2 and **FUC-Se** were built by Avogadro Soft [6] and Automated Topology Builder (ATB) Version 3.0[7], respectively. Three systems were constructed with number ratios (DSPE-PEG2: **FUC-Se**) of 0:35, 0:70 and 12:24 to systematically study the self-assemble behavior of **FUC-Se**. MD simulation was conducted using the GROMACS 19.5 package [8] with the gromos54a7_atb force field and SPCE explicit water model, and the system was electrically neutral by adding counterions. The boundary conditions were set to be periodic in x, y, and z directions. Energy minimization (1000.0 kJ/mol/nm) of all systems were implemented in the 2000 steps using the steepest descent method. Subsequently, NVT (300K, 1 ns) and NPT (1.0 bar, 2 ns) simulation were performed to achieve constant temperature and constant pressure of complex system. V-rescale [9] and Parrinello-Rahman protocol [10] were used to control the temperature and pressure of complex system, respectively. After that, 100 ns production simulations were performed. All bonds containing hydrogen atoms were constrained using the default linear constraint (LINCS) solver algorithm [11]. The Particle-Mesh Ewald (PME) method was employed to deal with long-range interactions, and a 10 Å cutoff was used for Van der Walls interactions [12]. The time step was 2 fs, and a snapshot was collected every 1.0 ps. After MD simulation, the GROMACS package (version 19.5) was used to analyze the trajectories, and the gmx Hbond program was used and predict the potential H-bond number.

5. *In vitro* and intracellular reactive oxygen species detection assay

(1) Singlet oxygen detection

SOSG was adopt as fluorescence probe for both *in vitro* and intracellular singlet oxygen detection. Refer to the reported literature [13] for detailed operation methods. For **FUC-Se** aqueous solution, 808 nm laser, 100 mW cm^{-2}, 30 min; For comparison of *in vitro* singlet oxygen generation between **FUC-Se** and **FUC-Se@LP**, 808 nm laser, 100 mW cm^{-2}, 6 min; For intracellular **FUC-Se@LP**, 808 nm laser, 100 mW cm^{-2}, 5 min. Electron spin resonance (ESR) spectroscopy was employed as a direct method to confirm $^1O_2$ generation. Aqueous samples containing **FUC-Se@LP** and the spin trap 2,2,6,6-tetramethylpiperidine (TEMP, 50 mM) were irradiated with an 808 nm laser (100 mW cm^{-2}) for 10 min at room temperature. ESR spectra were immediately recorded on a Bruker EMXplus-6/1 spectrometer.

(2) Superoxide anion detection

DHR123 and DHE were used for *in vitro* and intracellular superoxide anion detection, respectively. Refer to the reported literature [14] for detailed operation methods. For comparison of *in vitro* superoxide anion generation between **FUC-Se** and **FUC-Se@LP**, 808 nm laser, 100 mW cm^{-2}, 7 min; For intracellular **FUC-Se@LP**, 808 nm laser, 100 mW cm^{-2}, 5 min. ESR spectroscopy with spin trapping was used to directly verify $O_2^{-\bullet}$generation. Aqueous samples containing **FUC-Se@LP** and the spin trap 5,5-dimethyl-1-pyrroline N-oxide (DMPO, 50 mM) were irradiated with an 808 nm laser (100 mW cm^{-2}) for 10 min at room temperature. ESR spectra were immediately recorded on a Bruker EMXplus-6/1 spectrometer.

6. *In vitro* photothermal heating test and photothermal conversion efficiency calculation

(1) **FUC-Se** in DMSO and **FUC-Se** aqueous solution with same concentration (50 μM) were prepared, and then irradiated with 808 nm laser (0.5 W cm^{-2}) for 5 min. The temperature changes were recorded by infrared thermal camera (FLIR T420).

(2) **FUC-Se** and **FUC-Se@LP** aqueous solution with various concentration (10 μM, 30 μM, 50 μM, 70 μM) were prepared, and then irradiated with 808 nm laser (0.8 W cm^{-2}) for 5 min. The temperature changes were recorded by infrared thermal camera (FLIR T420).

(3) **FUC-Se** and **FUC-Se@LP** aqueous solution (50 μM) were prepared, and then exposed to 808 nm laser irradiation with various power density (0.33 W cm^{-2}, 0.6 W cm^{-2}, 0.8 W cm^{-2}, 1.0 W cm^{-2}) for 5 min. The temperature changes were recorded by infrared thermal camera (FLIR T420).

(4) To measure the photothermal conversion efficiency of **FUC-Se@LP**, **FUC-Se@LP** aqueous solution (50 μM) was exposed to 808 nm laser irradiation (1.0 W cm^{-2}) for 5 min, and then the solution cools naturally to room temperature. Note that from the beginning of turning off the laser, the temperature of the solution was recorded every 30 s with an infrared thermal camera. The photothermal conversion efficiencies (η) was measured according to the following formula:

$$\eta = \frac{hs(T_{Max} - T_{Surr}) - Q_{Dis}}{I(1 - 10^{-A})}$$

Where h is the heat transfer coefficient, s is the surface area of the container, Q_{Dis} represents heat dissipated from the laser mediated by the solvent and container. I is the laser power and A is the absorbance at 808 nm.

$$hs = \frac{mC}{\tau_s}$$

Where m is the mass of the solution, C is the specific heat capacity of the solution, and τ_S is the associated time constant.

$$t = -\tau_s \ln \theta$$

Where θ is a dimensionless parameter, known as the driving force temperature.

$$\theta = \frac{T - T_{Surr}}{T_{Max} - T_{Surr}}$$

Where T_{Max} and T_{Surr} are the maximum steady state temperature and the environmental temperature, respectively.

7. Cellular uptake and sub organelle colocalization assays

(1) Typically, 4T1 cells were seeded into laser confocal cell-culture dishes. After 24 h incubation, the culture medium was replaced with the fresh medium containing **FUC-Se** (5 μM) or **FUC-Se@LP** (5 μM). Confocal images were taken at specific moments after fresh medium addition (30, 60, 120, 180, and 240 minutes).

(2) 4T1 cells were plated onto 35 mm confocal dishes and incubated for 24 h. Then, after cells were co-cultivated with **FUC-Se** (5 μM) at 37 °C for 3 h, the cells were further stained by MitoTracker TMRM (300 μM). Fluorescence imaging was then carried out with a spectral confocal microscope (Olympus, FV3000), using a 60 × objective oil lens. The parameters were set as follows: **FUC-Se**, Ex = 635 nm, Em = 700-800 nm; MitoTracker TMRM, Ex = 559 nm, Em = 570-650 nm.

8. Evaluation of photo and dark toxicity of FUC-Se@LP under normoxia and mild hypoxia atmosphere

(1) Normoxia atmosphere (21% O_2 and 5% CO_2): 4T1 cells were seeded onto 96-well plates with 10^4 cells per well, and then were incubated at 37 °C under normoxia atmosphere for 24 h. Then, the original medium was removed and cells were washed with PBS twice. Subsequently, the fresh medium containing **FUC-Se@LP** at a serial of concentrations (0.5, 1.25, 2.5, 5.0 and 7.5 μM) was readded to the 96-well plate followed by another 3 h incubation. Afterwards, the cells were exposed to 808 nm laser (150 mW cm^{-2}, 10 min) under normoxia atmosphere. Next, the cells were further incubated for 12 h at 37 °C and then subjected to standard MTT procedures. Finally, the absorbance of 490 nm was measured with a Bio-Rad microplate reader and the cell viability was calculated by the following equation:

cell viability (%) = $(OD_{PS}-OD_{blank}) / (OD_{Contro}-OD_{blank})\times 100\%$

(2) Hypoxia atmosphere (10% O_2 and 2% O_2): 4T1 cells were seeded onto 96-well plates with 104 cells per well followed by 16 h incubation at 37 °C under normoxia atmosphere. To mimic different levels of tumor hypoxia, cells were then transferred into a humidified hypoxia chamber (MIC-101, Billups-Rothenberg) equilibrated with either 10% O_2 + 5% CO_2 (mild hypoxia) or 2% O_2 + 5% CO_2 (severe hypoxia). The oxygen level inside the chamber was monitored with an oxygen detector (Nuvair O2 Quickstick).. After another incubation for 8 h under mild hypoxia atmosphere, **FUC-Se@LP** was added at the same concentration gradient as above and incubated with the cells for 3 h under hypoxic

conditions. The subsequent laser irradiation and MTT procedures were identical to those performed under normoxic conditions.

For dark toxicity measurement, under both normoxic and mildly hypoxic conditions, light irradiation was not conducted during the experiment process, and all other steps were the same to those of phototoxicity tests.

9. Detection of immunogenic cell death biomarkers

(1) Immunofluorescence imaging of CRT and HMGB1: 4T1 cells were seeded on confocal cell-culture dishes (1×10^5 cells per well) followed 24 h of cell incubation at 37 °C in a humidified, 10% O_2 and 5% CO_2 atmosphere. Then, the cells were subjected to different treatments: a) without any treatments (Blank), b) only subjected to 808 nm laser irradiation (808 nm), c) only incubated with 5.0 μM **FUC-Se@LP** for 3 h (**FUC-Se@LP**), d) incubated with 5.0 μM **FUC-Se@LP** for 3 h and then irradiated with 100 mW cm^{-2} 808 nm laser for 4 min (**FUC-Se@LP** + 808 nm). After another 3h incubation, the medium was removed; cells were washed with PBS twice, and subsequently subjected to a series of immunofluorescence related sample pretreatment and staining operations, including fixing (4% paraformaldehyde, 37 °C, 1h), blocking (37 °C, 1h) and incubating with the primary antibody (4 °C, dark, overnight) and staining with the secondary antibody (dark, 37 °C, 2h) and Hoechst 33342 (500 nM, dark, 37 °C, 20 min) to tab cell membrane and nucleus. Finally, cells in each group were washed three times with PBS and immediately subjected to confocal luminescence imaging. The primary antibody: Calreticulin Rabbit Monoclonal Antibody for CRT detection and HMGB1 Rabbit Monoclonal Antibody for HMGB1 detection. The secondary antibody is Alexa Fluor 488-labeled Goat Anti-Rabbit IgG.

(2) Extracellular release of adenosine triphosphate (ATP): The cell culture and treatment protocols were identical to those described above. After another 3h incubation, the medium was collected and centrifuged at 4 °C for 5 min (12000 g), and the supernatant was collected and placed on ice, which was the sample to be tested. According to the instruction of the enhanced ATP test kit, standard samples were prepared and the working curve was measured. Finally, RUL value was detected by multi-function microplate reader, and ATP content in supernatant was statistically analyzed according to standard curve. Note: in order to reduce the interference between adjacent wells, the black 6-well plates were used in the experiment.

10. Animal welfare and Tumor model

The experimental BALB/c nude mice (female, 4–6 weeks) were purchased from Laboratory Animal Center of Dalian Medical University. All the animal experiments conducted in this work were approved

by the local research ethics review board of the Animal Ethics Committee of Dalian University of Technology (Certificate number//Ethics approval no. is 2018-043)

2×10^6 4T1 cells were dispersed in 100 μL of PBS and subcutaneously injected into BALB/c female mice (6 weeks) to establish a tumor-bearing model. Experiments on the mice commenced when tumor volumes reached about 200 mm^3.

11. *In vivo* biodistribution imaging

When tumors reached approximately 200 mm^3, **FUC-Se@LP** aqueous solution (60 μM) was *i.v.* injected into the mice. In vivo fluorescence imaging was carried out with the NIR-II In Vivo imaging system (In Vivo Master, Suzhou Yingrui Optical Technology Co., LTD) equipped with an InGaAs camera (λex =808 nm, long pass filter: 900 nm) at various time points. After 48 h post-injection of **FUC-Se@LP**, mice were sacrificed. Tumors and major organs (including hearts, livers, spleens, lungs, kidneys) were harvested and imaged for ex vivo fluorescence imaging to quantify the biodistribution of **FUC-Se@LP**.

12. *In vivo* anti-tumor in situ assays

When the subcutaneous 4T1 tumors reached approximately 200 mm^3, the mice were randomly divided into four groups with 5 mice in each group. **FUC-Se@LP** aqueous solution (60 μM, 200 μL) was *i.v.* injected into the mice for 1 time. Treatment groups were: 1) PBS (200 μL), 2) 808 nm laser, 3) **FUC-Se@LP** (60 μM), 4) **FUC-Se@LP** (60 μM, 200 μL) plus 808 nm laser irradiation (0.8 W cm^{-2}, 10 min). The body weight and tumor volume were recorded every other day. The tumor volume was calculated following the equation below:

Tumor volume = $1/2 \times LW^2$, "L" referred to the long diameter of the tumor. "W" meant the short diameter of the tumor.

13. *In vivo* Anti-distal tumor effects

To determine whether **FUC-Se@LP** could trigger systemic antitumor immune responses under light and retrain the growth of distant tumors, we established a mouse bilateral tumor model. Firstly, 2×10^6 4T1 cells were subcutaneously injected the right armpit of the mice to produce the primary tumor, then after 5 days the left armpit of the mice was subcutaneously inoculated with the same amount of 4T1 cells as the distant tumor. When the primary tumor reached approximately 120 mm^3, the mice were randomly divided into four groups with 5 mice in each group. The primary tumors in each group were subjected to different treatments: 1) intratumor injection PBS (100 μL), 2) 808 nm laser, 3) intratumor injection **FUC-Se@LP** (60 μM, 100 μL), 4) intratumor injection **FUC-Se@LP** (60 μM, 100 μL) plus 808 nm laser irradiation (0.8 W cm^{-2}, 10 min). The body weight and tumor volume of primary and distant tumors were recorded every other day.

Table S1. Quantitative comparison of key performance parameters of our **FUC-Se** system with state-of-the-art J-aggregate phototheranostics.

(Reference)	System	Assembly Trigger	Features
J. Am. Chem. Soc. **2019**, 141, 49, 19221-19225.	FD-1080	DMPC induced conventional J-aggregation	~1360 nm ROS: Unknown η: Unknown High-resolution NIR-II vascular imaging
Adv. Mater. **2025**, 37, 2501184	MSDP NPs	DSPE-PEG-RGD induced J-aggregation + intramolecular charge transfer	~760 nm Type I ROS η: 45.21% Type I PDT + PTT Tumor pyroptosis
Aggregate (**2025**), 6: e70211.	Cyp-TPE NPs	Asymmetric molecules arranged in an alternating manner form J-aggregates	~800 nm Type I & II ROS η: 27% PDT+PTT Tumor ferroptosis

Our work	FUC-Se	Zero-trigger (H_2O) CT Involved	~810 nm Type I & II ROS 0.139 η: 47.69% PDT/PTT/PIT

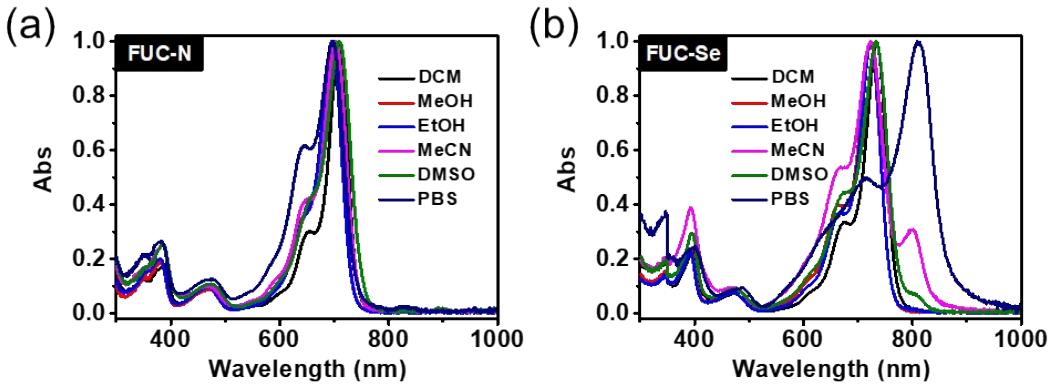

Figure S1. The normalized absorption spectra of (a) **FUC-N** and (b) **FUC-Se** in different solvents. The dye concentration is uniformly set at 1 μM.

Table S2. Photophysical parameters of **FUC-N** and **FUC-Se**.

	λ_{abs}[a] (nm)	λ_{em}[b] (nm)	ε[c]
FUC-N	709	722	12.6
FUC-Se	733	760	13.7

[a] Maximum absorption wavelength in DCM. [b] Maximum fluorescence emission wavelength in DCM. [c] Molar extinction coefficient in DCM, × 10^4 $M^{-1}cm^{-1}$.

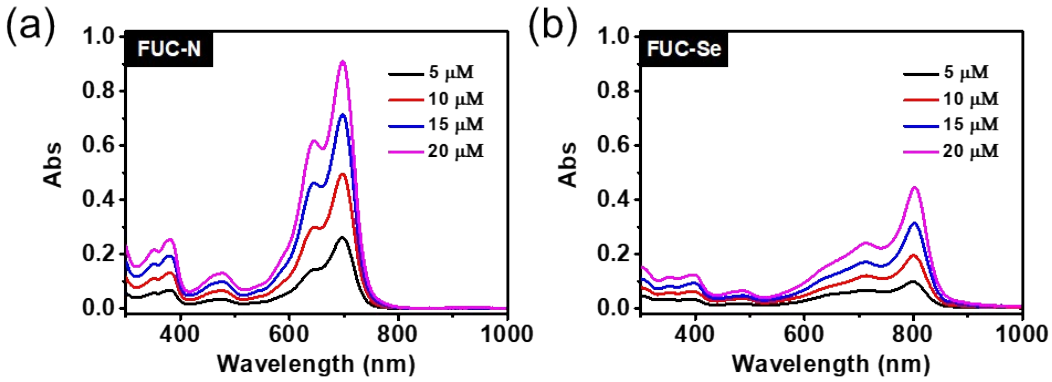

Figure S2. Absorption spectroscopy for (a) **FUC-N** and (b) **FUC-Se** with varied concentration in pure water. The dye was rapidly injected into the cuvette using a micropipette to initiate mixing. After a quick manual homogenization step (achieved by pipette mixing), spectral data collection was commenced without delay (< 5 s).

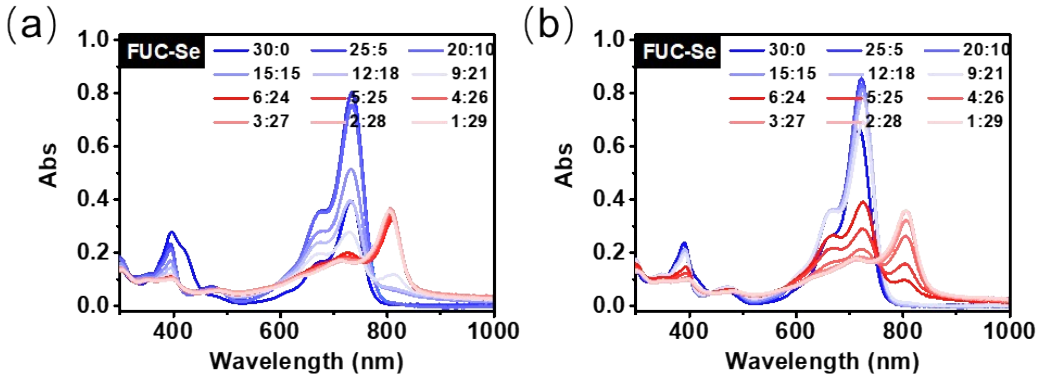

Figure S3. Variations in the absorption spectrum of **FUC-Se** across different ratios of mixed solvents. (a) EtOH/water; (b) DMSO/water.

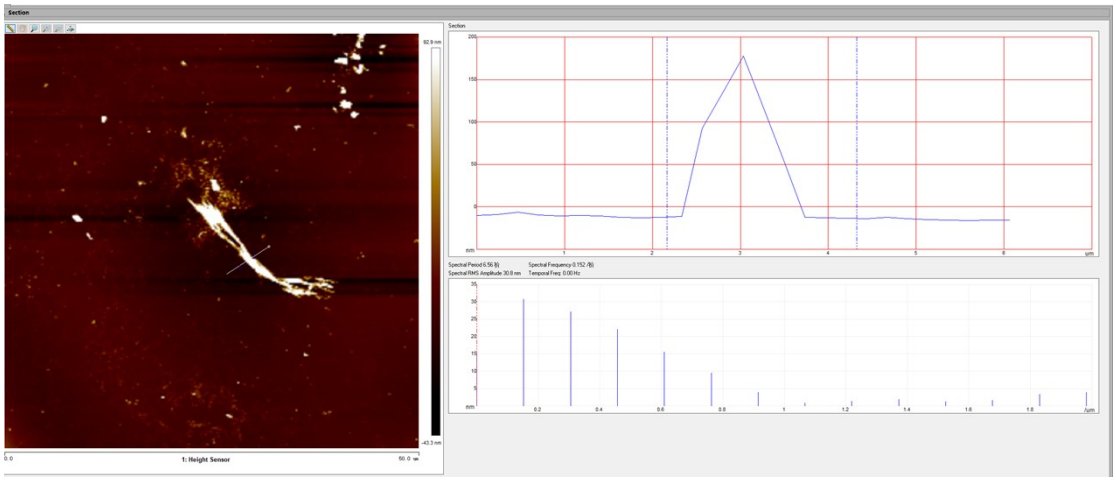

Figure S4. Atomic force microscopy (AFM) characterization of the **FUC-Se** J-aggregates.

Table S3. Crystal data and structure refinements of **FUC-Se** at 100 K.

Compound	**FUC-Se**
Empirical formula	$C_{34}H_{34}N_2O_5Se$
Formula weight	629.59
Temperature (K)	100(2)
Crystal system	monoclinic
Space group	$P2_1/c$
a (Å)	15.100(2)
b (Å)	32.293(5)
c (Å)	22.835(3)
α (°)	90
β (°)	106.375(6)
γ (°)	90
V (Å^3)	10683(3)
Z	12
D_c (g·cm^{-3})	1.174
μ (mm^{-1})	1.735
F (*000*)	3912
Crystal size (mm)	0.2 × 0.1 × 0.03
θ Range (°)	2.44 to 68.022
Reflections collected	162611
Independent reflections	13123/R_{int} = 0.0956
Data/restraints/parameters	18104/149/1154
GOF on F^2	1.042
R_1/wR_2 [$I > 2\sigma(I)$]	0.1314, 0.4375
R_1/wR_2 (all data)	0.1484, 0.4673
Max., Min. $\Delta\rho$ (e·Å^{-3})	1.673, -1.376
CCDC	2431831

Table S4. Hydrogen bonding parameters for **FUC-Se** at 100 K.

D-H···A	**D-H (Å)**	**H···A (Å)**	**D···A (Å)**	**< D-H···A**
O12-H12A···O8	0.84	2.09	2.66(11)	125
O13-H13···O9	0.84	1.84	2.66(12)	164
O15-H15···O2	0.84	1.87	2.71(11)	176
C27-H27···O12	0.95	2.54	3.24(13)	130
C33-H33B···O6^{i}	0.98	2.52	3.36(19)	143

C58-H58···O9	0.95	2.52	3.19(11)	128
C93-H93···O15	0.95	2.49	3.22(13)	133

Symmetry codes: i) 1 - *x*,1/2 + *y*,1/2 - *z*.

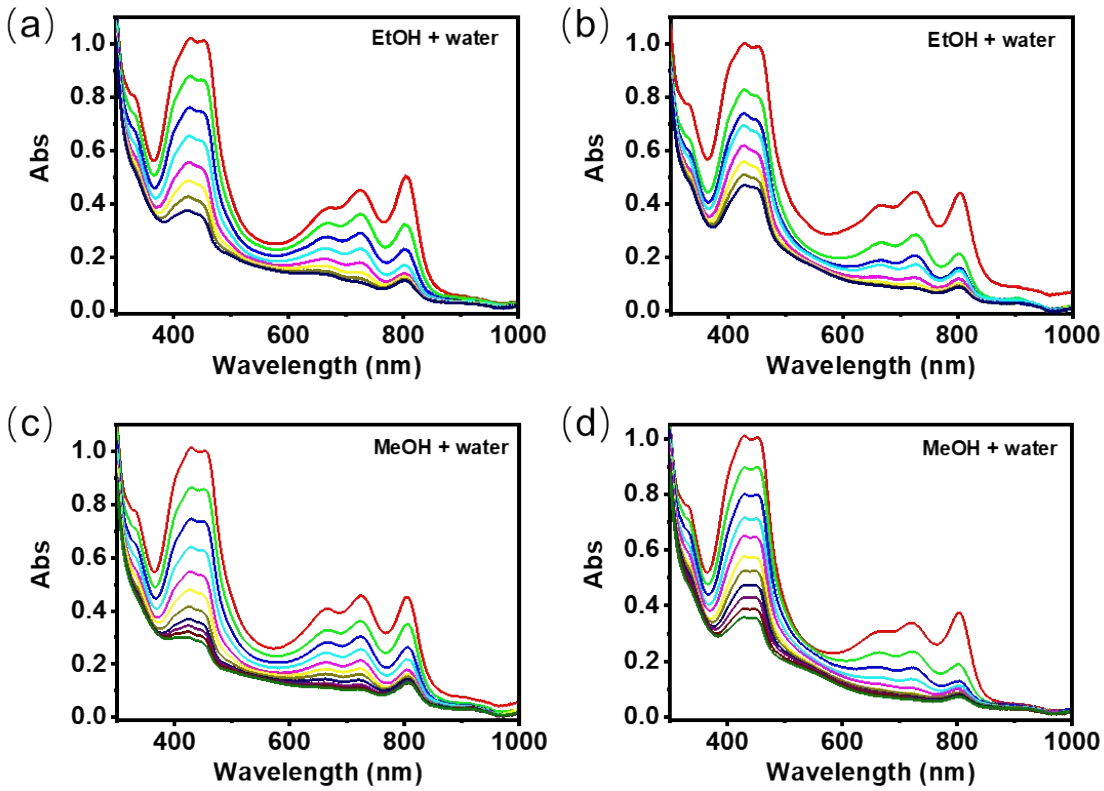

Figure S5. DPBF decay curves of **FUC-Se** in mixed system under laser irradiation (100 mW cm^{-2}). (a, b) In ethanol/water under 700 nm (a) and 808 nm (b) irradiation. (c, d) In methanol/water under 700 nm (c) and 808 nm (d) irradiation.

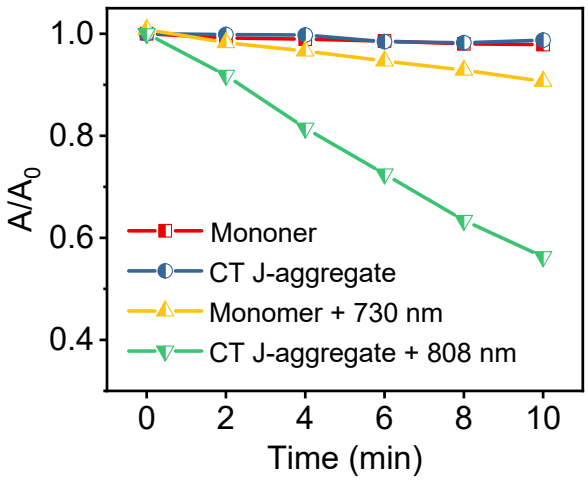

Figure S6. Complementary validation of singlet oxygen generation using ABDA degradation. Time-dependent absorption changes of ABDA (at 380 nm) were monitored under laser irradiation in the presence of **FUC-Se** monomers (700 nm, 100 mW cm^{-2}) or J-aggregates (808 nm, 100 mW cm^{-2}).

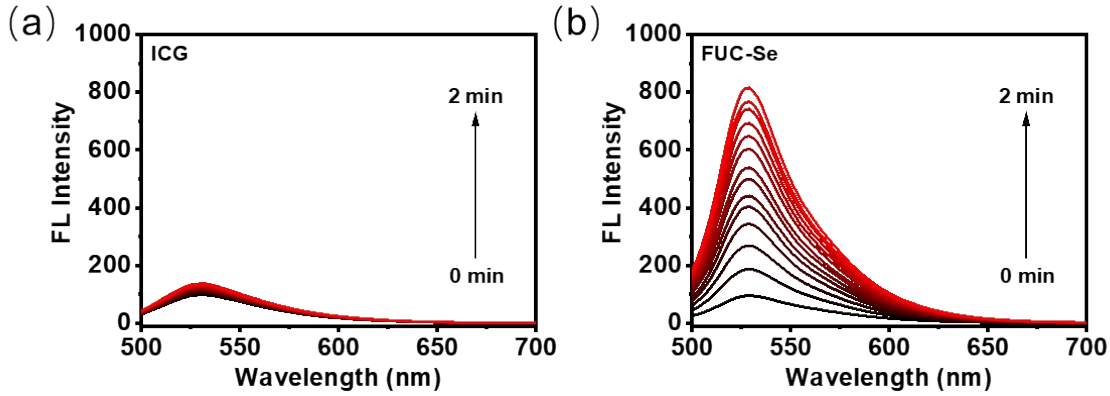

Figure S7. SOSG curves of (a) ICG and (b) **FUC-Se** in aqueous solution under 808 nm laser irradiation (100 mW cm^{-2}).

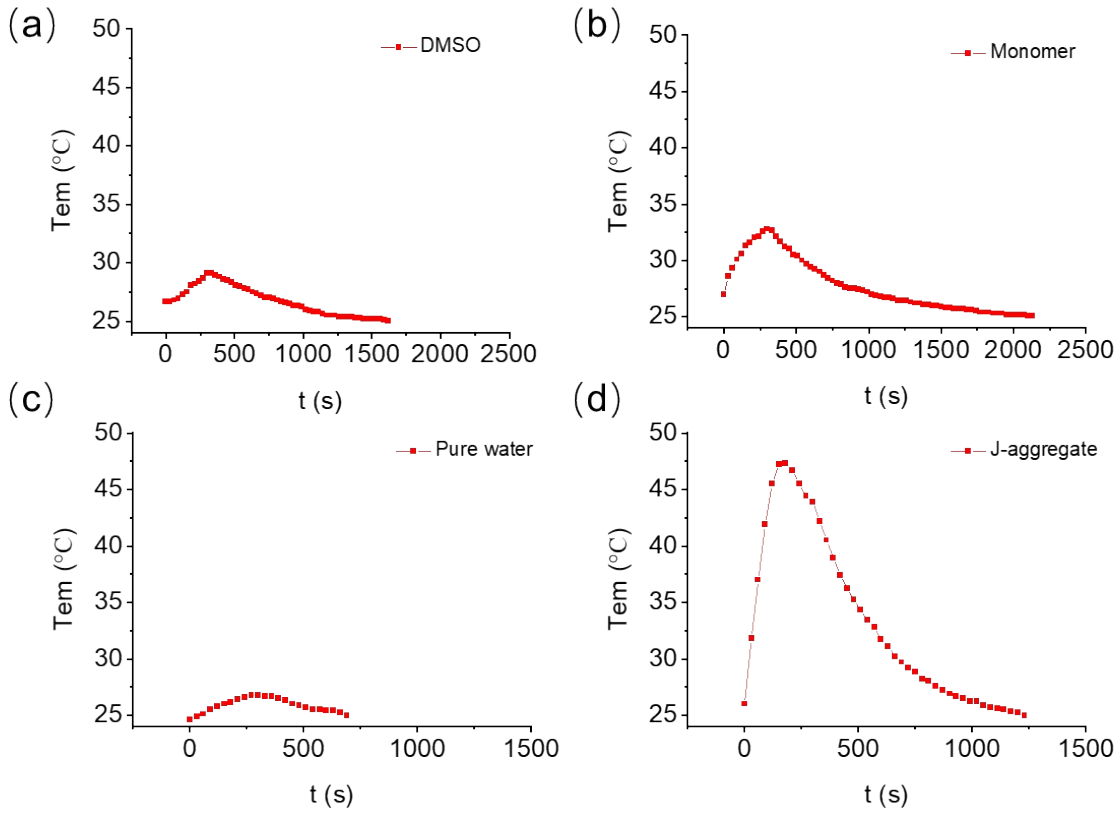

Figure S8. Rise and nature cooling curve of (a) DMSO, 700 nm, 0.5 W cm^{-2}, (b) **FUC-Se** monomer, 50 μM, 700 nm, 0.5 W cm^{-2}, (c) Pure water, 808 nm, 0.5 W cm^{-2}, (d) **FUC-Se** J-aggregate, 50 μM, 808 nm, 0.5 W cm^{-2}. All samples were adjusted to identical absorbance and irradiated under the same laser power density.

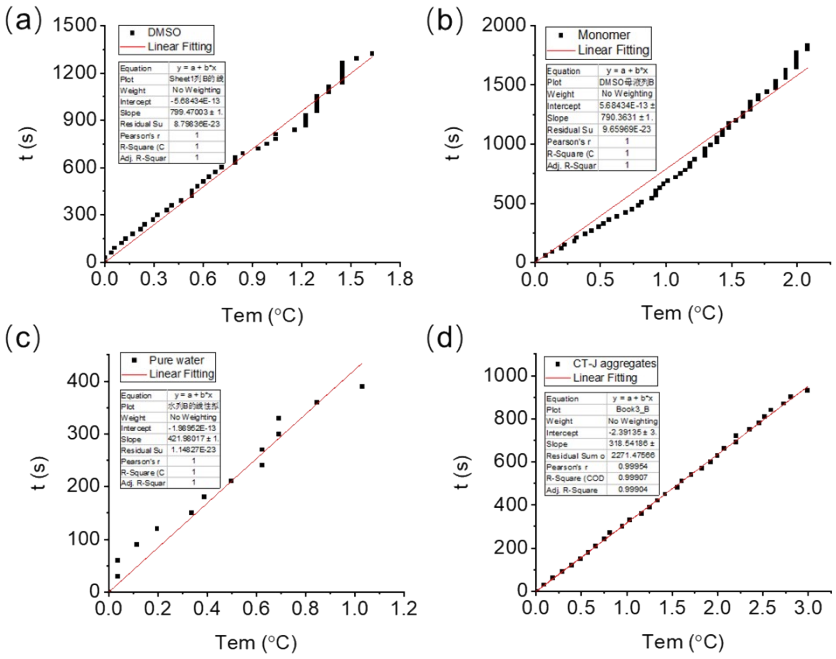

Figure S9. Time constant (τ_s) of (a) DMSO, (b) **FUC-Se** monomer, (c) Pure water, (d) **FUC-Se** J-aggregate.

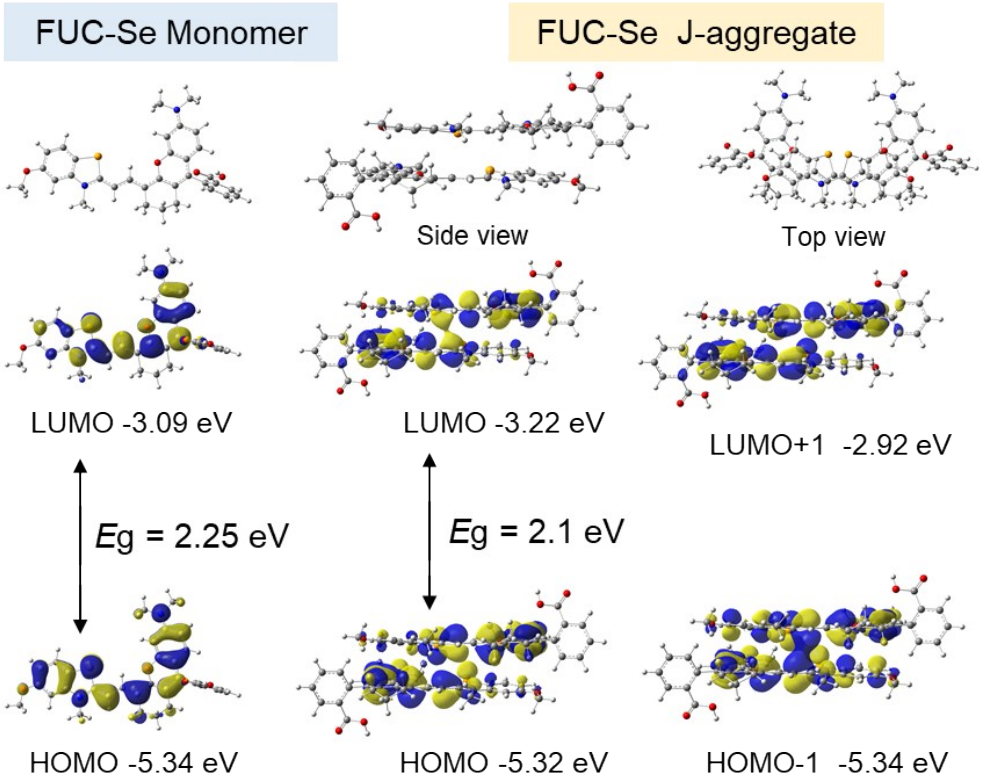

Figure S10. Calculated frontier molecular orbitals and energy gaps of **FUC-Se** monomer and its dimer, where the geometry of the dimeric motif is taken from the crystal packing of **FUC-Se**.

Table S5. The calculated excitation properties of **FUC-Se** monomer based on S0 geometry using TD-DFT at the B3LYP/TZVP level of theory together with PCM model.

Ex. state	transition	Cal/λ/nm	Cal/E/eV	f	Exp/ λ/nm
S1	HOMO→LUMO	686	1.806	1.3362	723
S2	HOMO-1→LUMO	486	2.649	0.2479	486
S3	HOMO→LUMO+1	442	2.802	0.0008	400

Table S6. The calculated excited states properties of **FUC-Se** monomer based on S0 geometry using TD-DFT at the B3LYP/TZVP level of theory together with PCM model.

Ex. state	transition	Cal/λ/nm	Cal/E_{em}/eV	*f*	Exp/ λ/nm
S1	HOMO→LUMO	728	1.701	1.3362	748
S2	HOMO-1→LUMO	478	2.592	0.2479	
T1	HOMO→LUMO	1112	1.115	0.3337	

Table S7. The calculated excitation properties of **FUC-Se** J-dimmer based on S0 geometry using TD-DFT at the B3LYP/TZVP lev-el of theory together with PCM model.

Ex. state	transition	Cal/λ/nm	Cal/E/eV	f	Exp/ λ/nm
S1	HOMO→LUMO	760	1.631	1.1658	808
S2	HOMO-1→LUMO	759	1.632	0.1430	
S3	HOMO→LUMO+1	630	1.967	0.3337	

Table S8. The calculated excited states properties of the **FUC-Se** J-dimmer based on S0 geometry using TD-DFT at the B3LYP/TZVP level of theory together with PCM model.

Ex. state	transition	Cal/λ/nm	Cal/E_{em}/eV	f	Exp/ λ/nm
S1	HOMO→LUMO	900	1.378	0.1444	
S2	HOMO-1→LUMO	760	1.629	1.0689	
S3	HOMO→LUMO+1	670	1.851	0.9869	
T1	HOMO→LUMO (87%) HOMO→LUMO+1(12%)	1061	1.125		
T2	HOMO-1→LUMO (72%) HOMO→LUMO+1(27%)	1043	1.240		

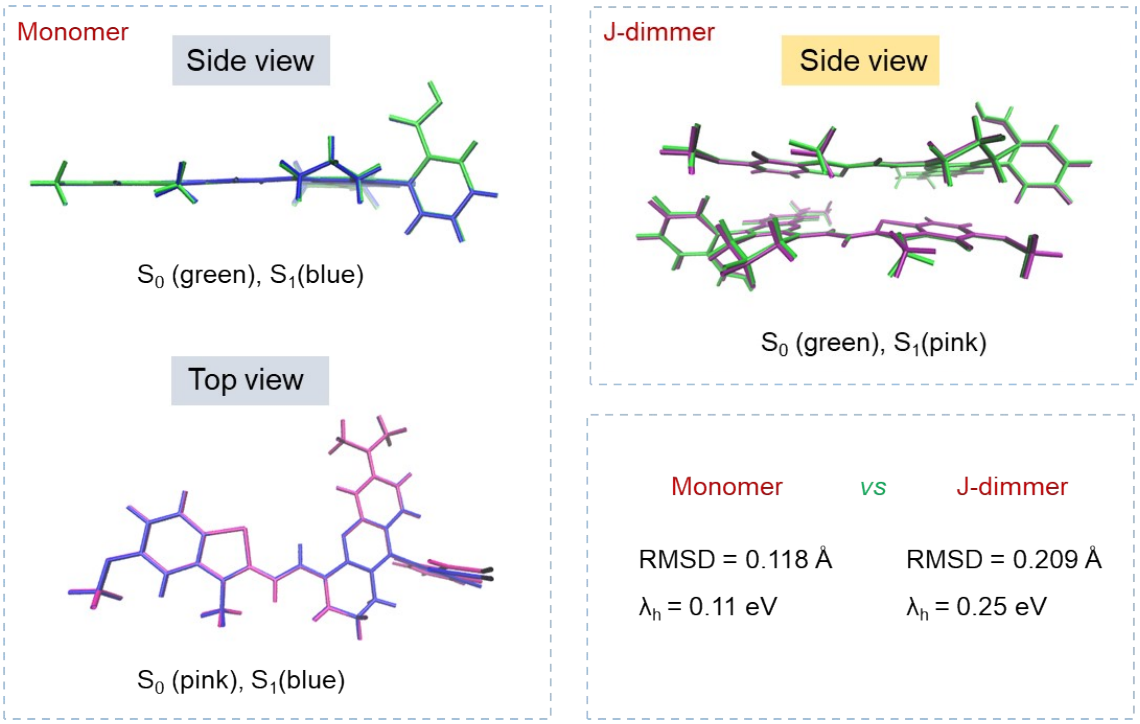

Figure S11. Overlay of the ground state and excited state structures of **FUC-Se** monomer and J-dimer with the root-mean-square deviation (RMSD) and reorganization energy (λ_h) (top view and side view).

Table. S9 Particle sizes of **FUC-Se@LP** prepared under different formulations.

$m_{DSPE-PEG2K}/m_{FUC-Se}$	0 day	2th day	4th day	6th day	8th day
1:4	2623	4315	5994	2475	3186
1:3	2764	2721	2417	2383	2894
1:2	390	341	304	276	326
1:1	650	865	731	530	753
2:1	73	62	83	86	145
4:1	65	78.7	58	56	115
6:1	62	78.7	79	78	80
8:1	62	177	164	54	58
10:1	72	116	73	61	57
12:1	60	68	53	49	45
15:1	75	81	66	57	61
20:1	52	57	51	47	43

Table. S10 Zeta potential of **FUC-Se@LP** prepared under different formulations

$m_{DSPE-PEG2K}/m_{FUC-Se}$	0 day	2th day	4th day	6th day	8th day
1:4	-8.9	-8.3	-13	-11.6	-7.6
1:3	-8.8	-7.4	-15.8	-12.9	-8.8
1:2	-13	-13.3	-14.6	-10.1	-16
1:1	-22	-28.1	-16.2	-27.8	-23.5
2:1	-13	-13.5	-13.8	-11.6	-14.7
4:1	-25	-21.7	-20.9	-28.4	-24.1
6:1	-7.8	-10.4	-9.7	-9.8	-9.6
8:1	-8.6	-9.3	-8.9	-11.3	-9.7
10:1	-13	-21	-17.2	-14.6	-15.5
12:1	-12	-16.3	-12.4	-9.8	-10.9
15:1	-5.8	-4.6	-3.8	-7.7	-3.3
20:1	-11	-8.3	-7.8	-7.6	-6.4

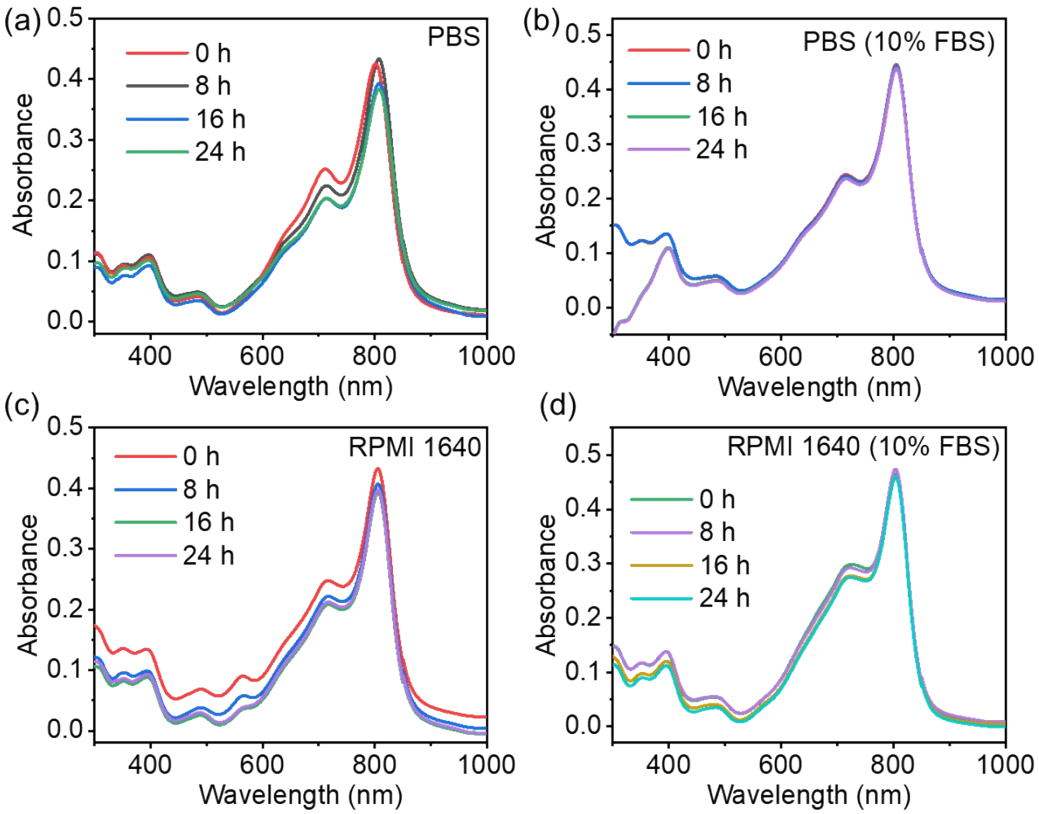

Figure S12. UV-Vis-NIR absorption spectrum of **FUC-Se@LP** nanoparticles in a biologically relevant medium over time. (a) PBS. (b) PBS + 10% FBS. (c) RPMI 1640. (d) RPMI 1640 + 10% FBS.

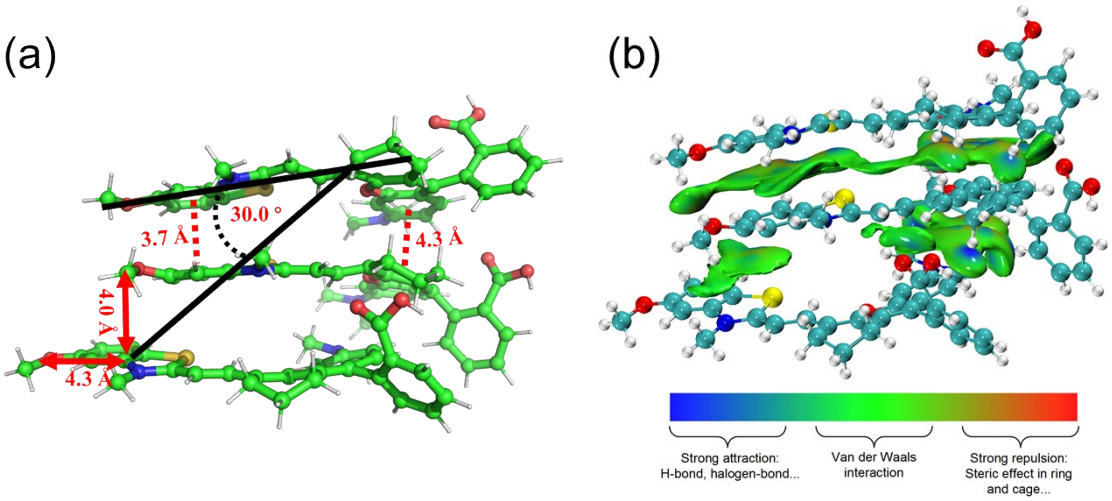

Figure S13. (a) Detail view of **FUC-Se** J-aggregates formed in DSPE-PEG2K. (b) IGM-plot iso-surface for **FUC-Se** J-aggregates from (a) (100 ns). Blue represents attractive or bonding interactions, green represents weak van der Waals interactions, and more green-colored atoms contribute more to the interaction, while red represents repulsive interactions.

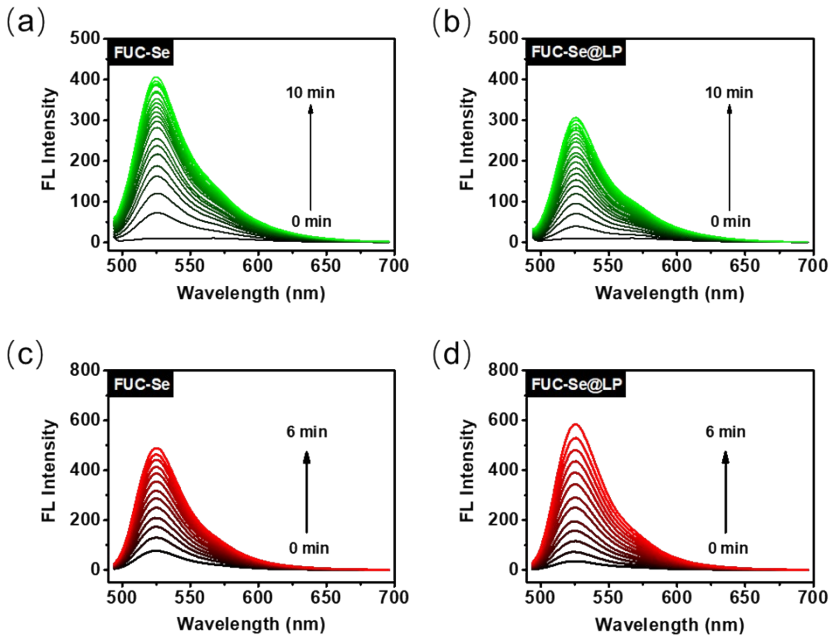

Figure S14. ROS production comparasion of **FUC-Se** and **FUC-Se@LP** under 808 nm irradiation. *In vitro* $^1O_2$ detection using SOSG as fluorescence probe (a) **FUC-Se** and (b) **FUC-Se@LP**; In vitro $O_2^{-\bullet}$ detection using DHR123 as fluorescence probe (c) **FUC-Se** and (d) **FUC-Se@LP**.

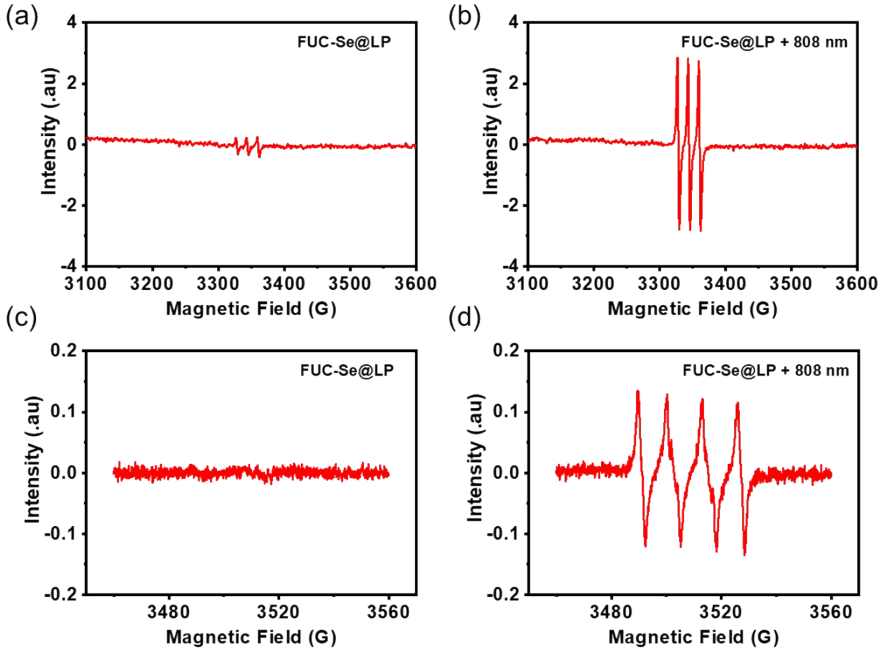

Figure S15. Electron spin resonance (ESR) spectroscopic analysis of reactive oxygen species (ROS) generation by **FUC-Se@LP**. (a, b) ESR spectra using TEMP as the spin trap for singlet oxygen: (a) in the dark and (b) upon 808 nm laser irradiation (100 mW cm^{-2}). The characteristic triplet signal in (b) confirms $^1O_2$ generation (Type-II pathway). (c, d) ESR spectra using DMPO as the spin trap for the superoxide anion radical ($O_2^{-\bullet}$): (c) in the dark and (d) upon the same laser irradiation.

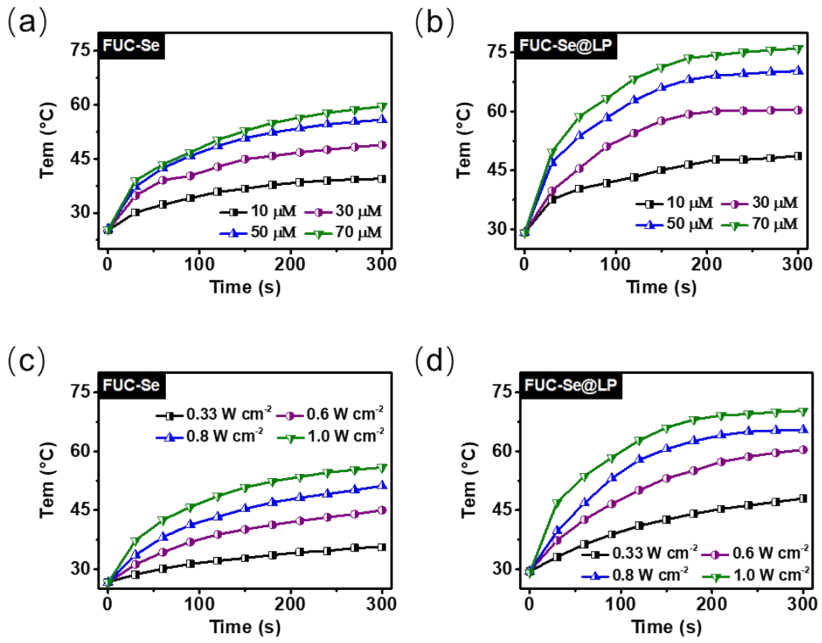

Figure S16. Photothermal property evaluation of **FUC-Se** and **FUC-Se@LP**. (a) Concentration-dependent and (c) laser power-dependent photothermal heating curve of **FUC-Se**. (b) Concentration-dependent and (d) laser power-dependent photothermal heating curve of **FUC-Se@LP**. laser power density, 808 nm, 1 W cm^{-2}, concentration, 50 μM.

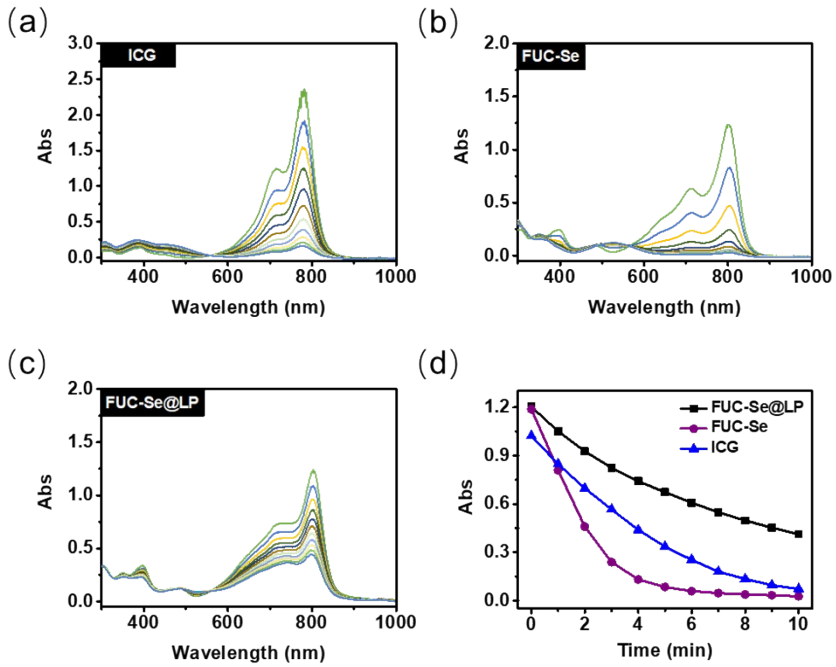

Figure S17. Photostability assay. Absorption spectral changes of (a) **FUC-Se**, (b) **FUC-Se@LP** and (c) **ICG** under 808 nm irradiation, 1W cm^{-2}, 50 μM; (d) Maxium absorbance changes as a function of light time.

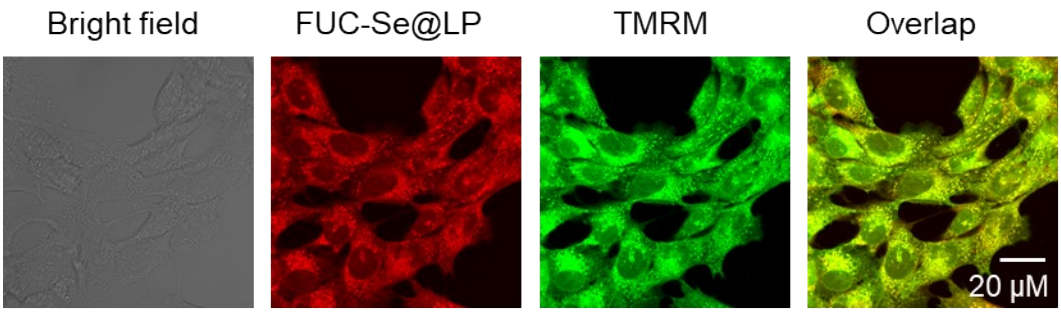

Figure S18. Laser confocal imaging of 4T1 cells incubated with **FUC-Se@LP** and mitochondrial localized dye TMRM.

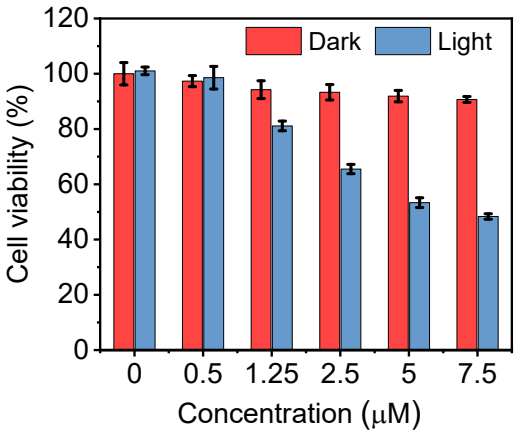

Figure S19. Photocytotoxicity of **FUC-Se@LP** in severe hypoxia (2% O_2 + 5% CO_2), 808 nm, 100 mW cm^{-2}, 5 min.

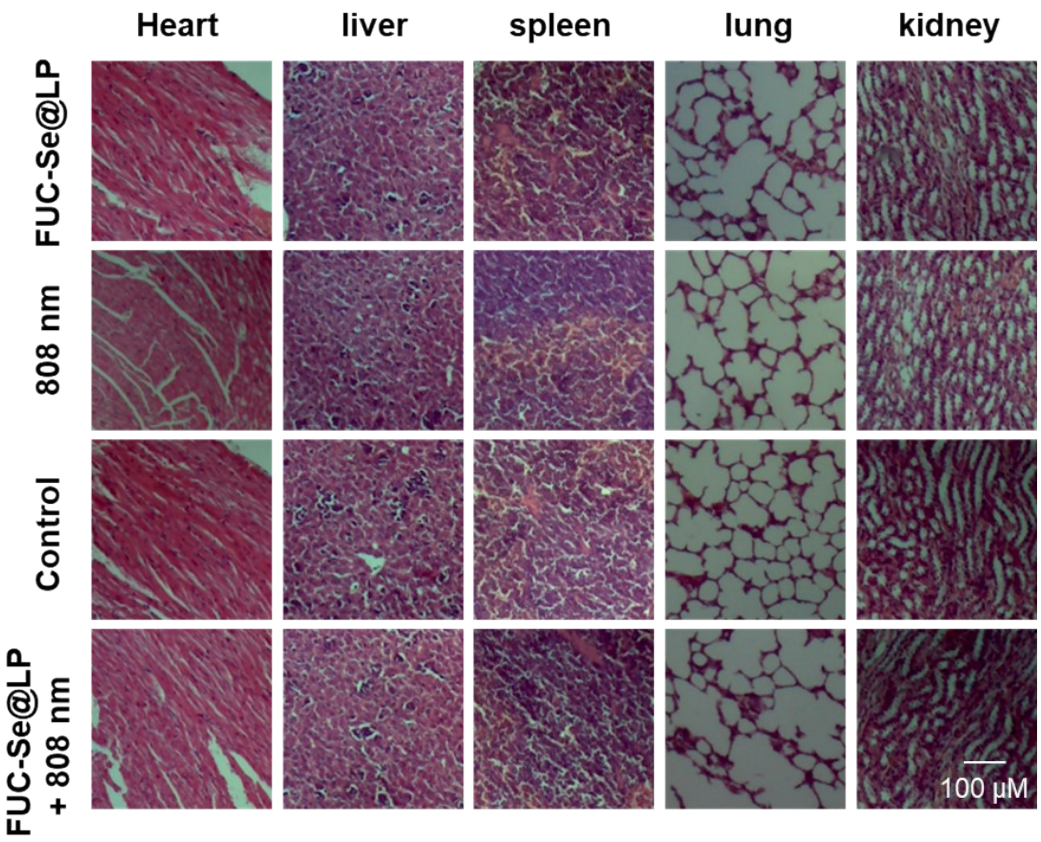

Figure S20. Histological analysis of major organs of mice from different treatment groups.

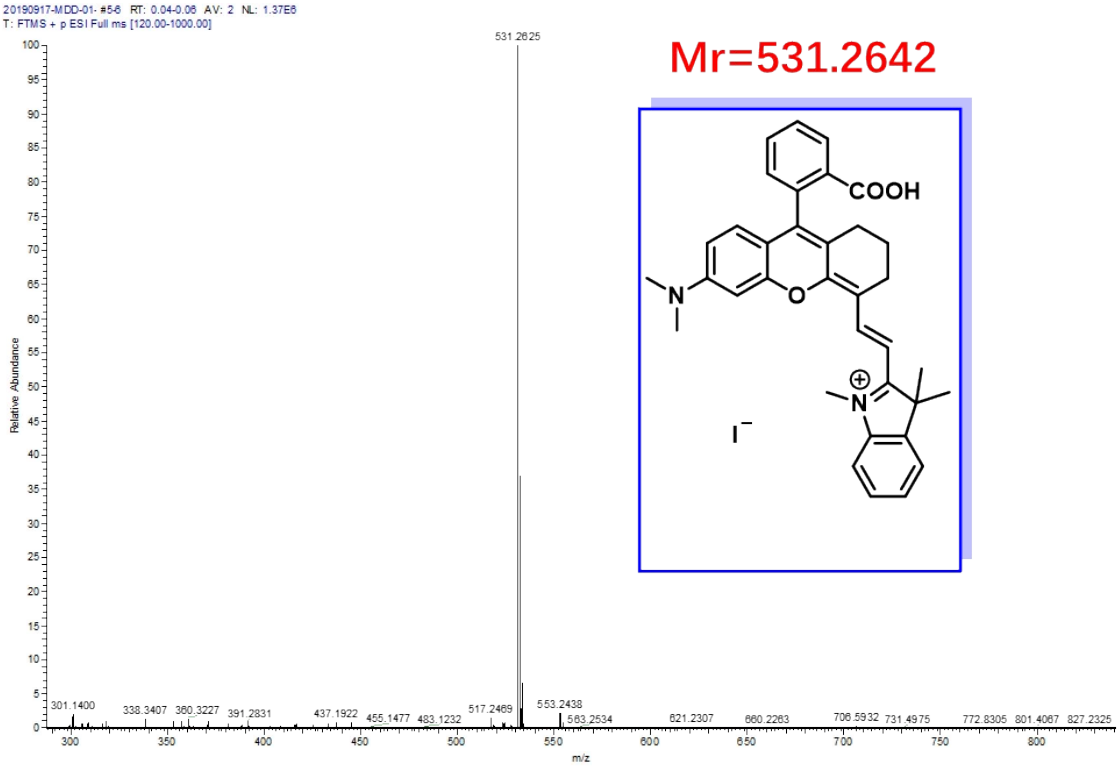

Figure S21. HRMS of **FUC-N**.

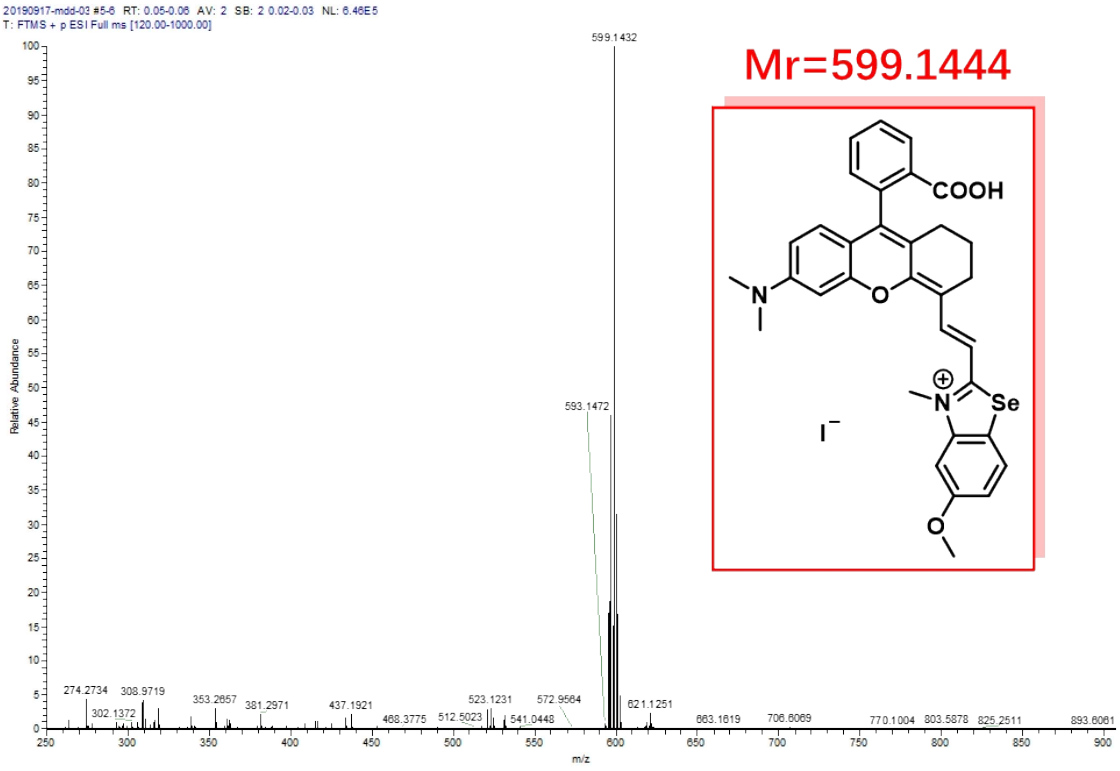

Figure S22. HRMS of **FUC-Se**.

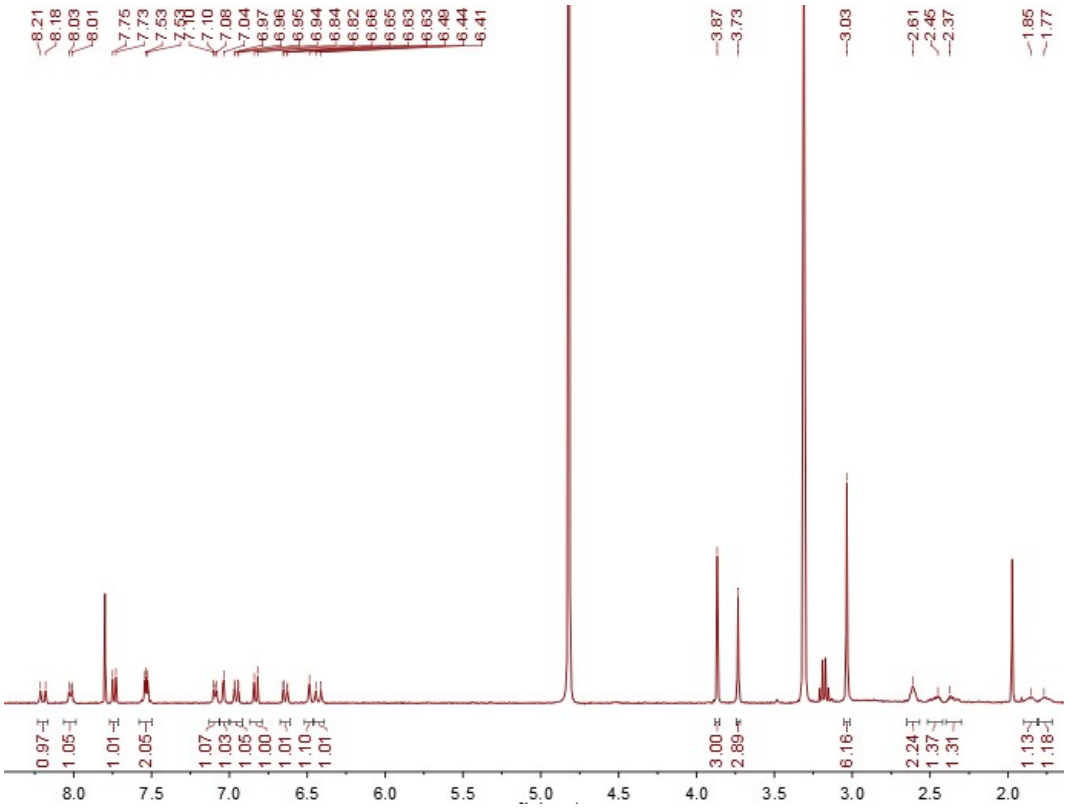

Figure S23. [1]HNMR of **FUC-Se**.

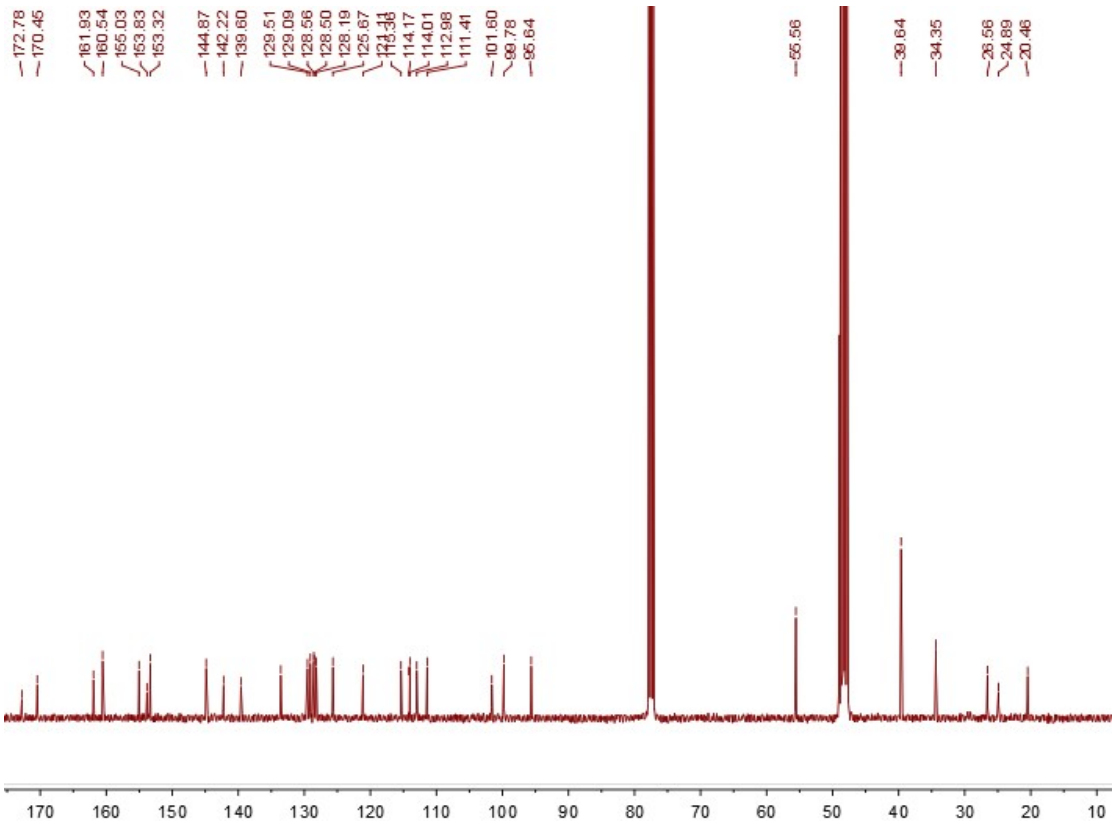

Figure S24. ^{13}CNMR of **FUC-Se**.

References.

1. A. V. Marenich, C. J. Cramer, D. G. Truhlar. Universal Solvation Model Based on Solute Electron Density and on a Continuum Model of the Solvent Defined by the Bulk Dielectric Constant and Atomic Surface Tensions. J. Phys. Chem. B. 2009, 113, 6378.
2. J. Tomasi, B. Mennucci and R. Cammi. Quantum Mechanical Continuum Solvation Models. Chem. Rev. 2005, 105, 2999
3. Frisch, M. J.; Trucks, G. W.; Schlegel, H. B.; Scuseria, G. E.; Robb, M. A.; Cheeseman, J. R.; Scalmani, G.; Barone, V.; Petersson, G. A.; Nakatsuji, H. et al. Gaussian 16 Rev. C.01; Gaussian, Inc.,Wallingford, CT, 2019.
4. Frank Neese. "Software Update: The ORCA Program System—Version 5.0". WIREs Comput Mol Sci. 2022;12: e1606.
5. Lu, T.; Chen, F. Multiwfn: A multifunctional wavefunction analyzer. J. Comput. Chem. 2012, 33, 580−592.
6. Gaussian 16, Revision C.01, Frisch, M. J.; Trucks, G. W.; Schlegel, H. B.; Scuseria, G. E.; Robb, M. A.; Cheeseman, J. R.; Scalmani, G.; Barone, V.; Petersson, G. A.; Nakatsuji, H.; Li, X.; Caricato, M.; Marenich, A. V.; Bloino, J.; Janesko, B. G.; Gomperts, R.; Mennucci, B.; Hratchian, H. P.; Ortiz, J. V.; Izmaylov, A. F.; Sonnenberg, J. L.; Williams-Young, D.; Ding, F.; Lipparini, F.; Egidi, F.; Goings, J.; Peng, B.; Petrone, A.; Henderson, T.; Ranasinghe, D.; Zakrzewski, V. G.; Gao, J.; Rega, N.; Zheng, G.; Liang, W.; Hada, M.; Ehara, M.; Toyota, K.; Fukuda, R.; Hasegawa, J.; Ishida, M.; Nakajima, T.; Honda, Y.; Kitao, O.; Nakai, H.; Vreven, T.; Throssell, K.; Montgomery, J. A., Jr.; Peralta, J. E.; Ogliaro, F.; Bearpark, M. J.; Heyd, J. J.; Brothers, E. N.; Kudin, K. N.; Staroverov, V. N.; Keith, T. A.; Kobayashi, R.; Normand, J.; Raghavachari, K.; Rendell, A. P.; Burant, J. C.; Iyengar, S. S.; Tomasi, J.; Cossi, M.; Millam, J. M.; Klene, M.; Adamo, C.; Cammi, R.; Ochterski, J. W.; Martin, R. L.; Morokuma, K.; Farkas, O.; Foresman, J. B.; Fox, D. J. Gaussian, Inc., Wallingford CT, 2016.
7. Cances, E.; Mennucci, B.; Tomasi, J. A New Integral Equation Formalism for the Polarizable Continuum Model: Theoretical Background and Applications to Isotropic and Anisotropic Dielectrics. *J. Chem. Phys.* **1997**, *107*, 3032–3041.
8. Mennucci, B.; Cances, E.; Tomasi, J. Evaluation of Solvent Effects in Isotropic and Anisotropic Dielectrics and in Ionic Solutions with a Unified Integral Equation Method: Theoretical Bases, Computational Implementation, and Numerical Applications. *J. Phys. Chem. B* **1997**, *101*, 10506–10517.

9. Miertus, S.; Scrocco, E.; Tomasi, J. Electrostatic Interaction of a Solute with a Continuum – A Direct Utilization of Abinitio Molecular Potentials for the Prevision of solvent Effect. *Chem. Phys.* **1981**, *55*, 117–129.
10. Cammi, R.; Tomasi, J. Remarks on the Use of the Apparent Surface-Charges (ASC) Methods in Solvation Problems – Iterative Versus Matrix-Inversion of the Apparent Charges. *J. Comput. Chem.* **1995**, *16*, 1449–1458.
11. Grimme, S.; Ehrlich, S.; Goerigk, L. Effect of the damping function in dispersion corrected density functional theory. *J. Comp. Chem.* **2011,** *32,*1456-1465.
12. Gao, X.; Bai, S.; Fazzi, D.; Niehaus, T.; Barbatti, M.; Thiel, W. Evaluation of Spin-Orbit Couplings with Linear-Response TimeDependent Density Functional Methods. *J. Chem. Theory Comput.* **2017,** *13,* 515−524.
13. Mingle Li, Jing Xia, Ruisong Tian, Jingyun Wang, Jiangli Fan, Jianjun Du, Saran Long, Xiangzhi Song, James W. Foley, and Xiaojun Peng. Near-Infrared Light-Initiated Molecular Superoxide Radical Generator: Rejuvenating Photodynamic Therapy against Hypoxic Tumors. *J. Am. Chem. Soc.* **2018**, 140, 14851−14859.
14. He Ma, Yang Lu, Zhibin Huang, Saran Long, Jianfang Cao, Zhen Zhang, Xiao Zhou, Chao Shi, Wen Sun, Jianjun Du, Jiangli Fan, and Xiaojun Peng*. ER-Targeting Cyanine Dye as an NIR Photoinducer to Efficiently Trigger Photoimmunogenic Cancer Cell Death. *J. Am. Chem. Soc.* **2022**, 144, 3477−3486.